Applied Catalysis B: Environmental 142–143 (2013) 677–683

Contents lists available at SciVerse ScienceDirect

Applied Catalysis B: Environmental

journal homepage: www.elsevier.com/locate/apcatb

Comparison of the performance for oxidation of formaldehyde on nano-Co_3O_4, 2D-Co_3O_4, and 3D-Co_3O_4 catalysts

Bingyang Bai, Hamidreza Arandiyan, Junhua Li*

State Key Joint Laboratory of Environment Simulation and Pollution Control, School of Environment, Tsinghua University, Beijing 100084, China

ARTICLE INFO

Article history:
Received 3 February 2013
Received in revised form 26 April 2013
Accepted 22 May 2013
Available online 13 June 2013

Keywords:
Co_3O_4
Formaldehyde
Catalytic combustion
Hard template
Three-dimensional channel

ABSTRACT

2D-Co_3O_4 and 3D-Co_3O_4 catalysts were prepared by the hard template method, and nano-Co_3O_4 was synthesized by precipitation method. The catalytic activity for the oxidation of formaldehyde over various types of catalysts was investigated. The 3D-Co_3O_4 catalyst attained a 100% conversion rate of formaldehyde at 130 °C with a space velocity of 30,000 mL/(g h), while the 2D-Co_3O_4 catalyst oxidized formaldehyde completely at 150 °C in the same space velocity conditions. The difference in activity is due to the clear channel structure of the mesoporous Co_3O_4 prepared by the hard template method, which has large specific surface area and surface active species that allows the reactant to diffuse and undergo surface reactions. The 3D-Co_3O_4 had the best performance of formaldehyde oxidation due to the three-dimensional porous channel structure, larger specific surface area, abundant active surface oxygen species and active Co^{3+} cationic species on the exposed (2 2 0) crystal face. Complete conversion of formaldehyde had remained the same after 3D-Co_3O_4 was observed for 160 h. Therefore, the 3D-Co_3O_4 catalyst has the best catalytic activity and stability for formaldehyde, which might be a non-noble catalyst for catalytic removal of formaldehyde in practical application.

1. Introduction

In recent years, much attention has been attracted to the control of volatile organic compounds (VOCs) from the chemical industry, building materials, coatings, motor vehicle, etc. Formaldehyde emitted from the widely used building and decorative materials is becoming a major indoor pollutant, and it also has photochemical activity in the atmosphere. Formaldehyde of low concentration in airtight buildings could cause serious and hazardous effects on human health. It has been deemed a carcinogenic and teratogenic substance [1,2]. Due to effects of human health and atmospheric environment, it is essential to remove and transfer to CO_2 in indoor air and industrial and automobile exhaust gas.

Porous materials with physical adsorption were used to eliminate formaldehyde emission, but the efficiency of removal was not excellent because of the limited capacities [2,3]. Catalytic combustion can be found to remove the formaldehyde for indoor air purification. This method has many advantages, such as high removal efficiency, a low light-off temperature, a wide range of applications, simple operation of equipment, and no secondary pollution. Currently, the catalytic materials used in formaldehyde catalytic oxidation are mainly oxide-supported precious metal catalysts, such as Pt/TiO_2 [2–4], Pt/MnO_2 [5], Pt/Fe_2O_3 [6], Pt/SiO_2 [7], Pt/MnO_x–CeO_2 [8], Ag/HMO [9], Ag/SBA-15 [10], Ag/SiO_2 [11], Ag/MnO_x–CeO_2 [12], Au/CeO_2 [13–15], Au/ZrO_2 [16], Au/Fe_2O_3 [17], Au/Co_3O_4–CeO_2 [18], Au/CeO_2–Co_3O_4 [19], Pd/TiO_2 [20], Pd/Beta [21] and Pd–Mn/Al_2O_3 [22]. In addition, perovskite type metal oxides as catalysts for the oxidation of formaldehyde have been reported [23]. The activity of supported noble metals (Pt, Ag, Au, Pd) is superior, but the high cost is prohibitive. Metal oxide catalysts are cheap, exhibit sufficient activity and are more practical. Catalytic materials with the same composition but different structure or morphology show diverse catalytic activity and expose the active site to varying extents [24,25].

Co_3O_4 demonstrates excellent catalytic performance and is widely used in various fields [26–28]. Co_3O_4 catalytic materials can have different morphologies, including tube, sheet, belt, rod, sphere and pore [29–31]. The reported results show that the different morphologies and structures of Co_3O_4 promote different chemical reactions and catalytic abilities because of the surface exposure of the active position. The research of Xie et al. [25] showed that CO can be easily oxidized by the sufficient Co^{3+} species exposed on the (1 1 0) face of a Co_3O_4 nano-rod. Hu et al. [29] synthesized nano-sheet, nano-belt and nano-cubic catalysts. The results indicated that the (1 1 2) face of the nano-sheet had excellent methane oxidation activity. Ma et al. [18] prepared catalysts with SBA-15 as a hard template. The results showed that the (1 1 0) face composed of Co^{3+} is active for the formaldehyde oxidation reaction and

* Corresponding author. Tel.: +86 10 62771093; fax: +86 10 62771093.
E-mail address: lijunhua@tsinghua.edu.cn (J. Li).

0926-3373/$ – see front matter © 2013 Elsevier B.V. All rights reserved.
http://dx.doi.org/10.1016/j.apcatb.2013.05.056

that oxidation ability is connected with the surface oxygen species. Therefore, it is meaningful and significant to research the characteristics of Co_3O_4 catalysts with the same components and different structures in the formaldehyde oxidation reaction and to investigate whether the three-dimensional porous channels of 3D-Co_3O_4 can increase the catalytic activity at low temperature. In this article, 2D-Co_3O_4, 3D-Co_3O_4 and nano-Co_3O_4 catalysts were prepared, and their structures were characterized by XRD, BET, TEM, O_2-TPD, H_2-TPR and XPS. The performance of the catalysts was evaluated in a microtype evaluation device to evaluate the activity of the mesoporous Co_3O_4 catalysts for the conversion of formaldehyde.

2. Experimental

2.1. Catalyst preparation

2.1.1. Synthesis of SBA-15 silica

SBA-15 was synthesized under acidic conditions using tetraethoxysilane (TEOS) as the silica source and Pluronic P123 ($EO_{20}PO_{70}EO_{20}$) as the structure-directing agent [32]. In a typical synthesis, P123 (8.0 g) was dissolved in 180 g of deionized water and 120 g of HCl (4 M) solution in a three-neck round-bottom flask with stirring. 9.1 mL of tetraethoxysilane (TEOS) was slowly added to the acid solution using a dropping funnel. The liquid mixture was stirred at room temperature for 24 h, and then it was transferred to a Teflon-lined stainless steel autoclave at 100 °C for 24 h. The white product was washed, air-dried at 100 °C and calcined at 550 °C for 5 h to completely eliminate the template. The resulting powder was two-dimensional SBA-15 molecule sieves.

2.1.2. Synthesis of KIT-6 silica

High quality mesoporous cubic (ia3d) silica material was synthesized using tetraethoxysilane (TEOS) as the silica source and Pluronic P123 ($EO_{20}PO_{70}EO_{20}$) as the structure-directing agent [33]. In a typical synthesis, P123 (1.2 mmol, 7.2 g), hydrochloric acid (37%, 13.9 g) and *n*-butanol (94.5 mmol, 7.0 g) were fed into a 500 mL round-bottom flask and stirred for 1 h. The temperature was kept at 38 °C in synthesis process. TEOS (7.0 g) was added, and the solution was stirred for another 24 h. The solution was transferred to a Teflon-lined stainless steel autoclave at 100 °C for 24 h. The mixture liquid was washed with deionized water and filtered several times after the hydrothermal treatment. The sample was dried at 100 °C and calcined at 550 °C for 5 h to completely eliminate the template. The white mesoporous KIT-6 was obtained.

2.1.3. Nanocasting preparation of mesoporous 2D-Co_3O_4 and 3D-Co_3O_4

Mesoporous Co_3O_4 was prepared using 2D porous SBA-15 and 3D porous KIT-6 as the hard template with ethanol as the dispersing agent. In a typical synthesis, 3.0 g of SBA-15 or KIT-6 molecular sieve were added to a $Co(NO_3)_2{\cdot}6H_2O$ ethanol solution (0.84 mol/L, 30 mL). The samples were evaporated to dryness at 80 °C. The products were calcined at 200 °C for 6 h. The above steps about casting and evaporating were repeated. Finally, the materials were calcined at 450 °C for 6 h. The SBA-15 and KIT-6 hard templates were removed using a 2 mol/L NaOH solution. Centrifugal separation was used to eliminate sodium silicate, and the samples were dried at 100 °C. The obtained powder was 2D-Co_3O_4 or 3D-Co_3O_4.

2.1.4. Preparation of nano-Co_3O_4

Nano-Co_3O_4 was prepared by the precipitation method [34]. A $Co(NO_3)_2{\cdot}6H_2O$ solution (0.37 mol/L, 20 mL) was slowly added to an Na_2CO_3 solution (1.25 mol/L, 8 mL). The mixture was stirred for 12 h and then washed, filtered, and dried at 100 °C. The resulting $Co(OH)_2$ was calcined at 400 °C for 4 h to obtain nano-Co_3O_4.

2.2. Catalyst characterization

XRD patterns were measured on a TTR3 type X-ray diffractometer using a Cu Kα ray radiation source with a 0.05°/min scanning speed, 40 kV tube voltage and 40 mA tube current. The 2θ of the low-angle XRD ranged from 0.6 to 5°, and the 2θ of the wide-angle ranged from 10 to 80°. The structural parameter, pore size distribution and N_2 adsorption isotherms of the samples were measured at liquid nitrogen temperature using an Autocorb-1MP apparatus. The samples underwent vacuum treatment at 300 °C for 4 h before testing. The N_2 adsorption–desorption isotherm used the Barrett–Joyner–Halenda (BJH) method. TEM image was taken on JEM-2011LaB6 instrument at a voltage of 200 kV. The samples were prepared by ultrasonic dispersion in ethanol and were dispersed for 8 min, and the transparent suspended droplets were placed on a copper grid using a capillary. The H_2-TPR was tested on a Chemisorb 2720 TPX apparatus using a temperature range of 50–900 °C with a heating rate of 10 °C/min. The catalysts were pretreated in the N_2 flow at 300 °C for 1 h in a quartz reactor prior to testing. The O_2-TPD was also measured on the above instrument. The catalysts were treated at 300 °C with 50 mL/min of He (5% of O_2) for 1 h. The samples adsorbed enough O_2 when the treatment temperature decreased below 80 °C, at which point the carrier gas was changed to pure He. The temperature was programmed to increase to 1000 °C at a rate of 10 °C/min. The XPS patterns were tested on a PHI-5300/ESCA electronic energy spectrum at 300 W using Mg Ka X-rays as the excitation source. The data were processed by the XPS-PEAK software.

2.3. Evaluation of catalytic activity

The catalytic oxidation activity on formaldehyde was tested in a fixed bed quartz tube reactor (Φ 10 mm) with 0.2 g catalyst (40–60 mesh). Formaldehyde gas was generated and injected using a N_2 bubbler in a low temperature thermostatic bath at 0 °C that passed through a container filled with formalin (an aqueous solution of 37% HCHO). The total flow rate through the reactor was kept at 100 mL/min by mass-flow meters and included 400 ppm formaldehyde, 20% (vol) of O_2 and N_2 equilibrium gas. The space velocity of the catalytic oxidation was 30,000 mL/(g h). The products of the reaction were analyzed online by an Agilent 7890A gas chromatograph with a TCD detector and a Porapak-Q column. No carbon products other than CO_2 were detected. The HCHO conversion was calculated from the CO_2 content as follows:

$$\text{HCHO conversion}\,(\%) = \frac{[CO_2]_{out}}{[HCHO]_{in}} \times 100$$

$[CO_2]_{out}$ and $[HCHO]_{in}$ in the formula are the CO_2 concentration in the products and the HCHO concentration of the flow gas, respectively.

3. Results and discussion

3.1. The activity of various catalysts for formaldehyde oxidation

The formaldehyde catalytic oxidation activities of the different Co_3O_4 catalysts are shown in Fig. 1. With an increase in temperature, the nano-Co_3O_4 catalyst displays the worst catalytic activity, completely converting HCHO at 230 °C, the 2D-Co_3O_4 catalyst has better oxidation activity, entirely converting HCHO at 150 °C, and the 3D-Co_3O_4 sample shows the best catalytic oxidation, entirely converting HCHO at 130 °C. The results indicate that the mesoporous materials have an advantage because of their structure. The three dimensional porous channels and the large surface area of the 3D-Co_3O_4 is highly conducive to formaldehyde oxidation. Fig. 2 shows HCHO catalytic activity of normalized by BET surface areas

Table 1
Porous structure parameter and surface composition of the different Co_3O_4 catalysts.

Sample	Surface area (m^2/g)		Pore volume	Pore diameter	Cobalt (mol%)		Oxygen (mol%)	
	A_{BET}	A_{BJH}	V_p (cm^3/g)	D_P (nm)	Co^{3+}	Co^{2+}	O_{ads}	O_{latt}
Nano-Co_3O_4	28.1	–	–	–	25.1	74.9	48.2	51.8
2D-Co_3O_4	43.3	48.8	0.013	4.78	32.9	67.1	46.1	53.9
3D-Co_3O_4	85.9	104.5	0.014	3.84	40.9	59.1	47.4	52.6

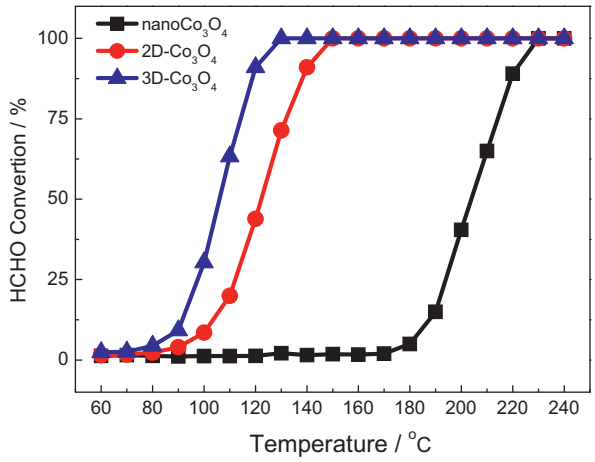

Fig. 1. Formaldehyde catalytic performance of the different Co_3O_4 catalysts under the following conditions: HCHO concentration = 400 ppm, 20 vol% O_2, N_2 as balance gas, GSHV = 30,000 mL/(g h).

(Table 1). It is observed that normalized activity of the 3D-Co_3O_4 is much better than the other catalysts after deducting surface areas. Fig. 3 shows the influence of airspeed for the formaldehyde catalytic activity of 3D-Co_3O_4 catalyst. From the chart, light-off temperature of formaldehyde gradually raises, with airspeed increasing from 30,000 mL/(g h) to 6,0000 mL/(g h). However, when space velocity reached 60,000 mL/(g h), the temperature of complete conversion of formaldehyde was at 160°C. This result indicates that the performance of 3D-Co_3O_4 is clearly influenced by space velocity. The formaldehyde catalytic performances with time on stream for different Co_3O_4 catalysts are displayed in Fig. 4. The conversion of formaldehyde had remained the same after these catalysts were observed for 160 h. The complete conversion of 3D-Co_3O_4 always kept at 130 °C. It indicates that the 3D-Co_3O_4 catalyst is highly stable in this condition.

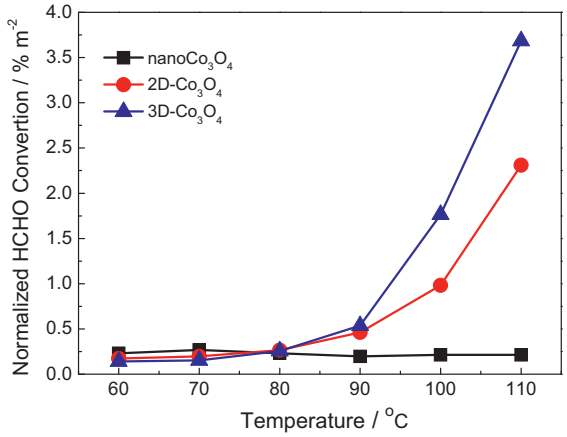

Fig. 2. Formaldehyde catalytic performance of the different Co_3O_4 catalysts normalized by BET surface area under the following conditions: HCHO concentration = 400 ppm, 20 vol% O_2, N_2 as balance gas, GSHV = 30,000 mL/(g h).

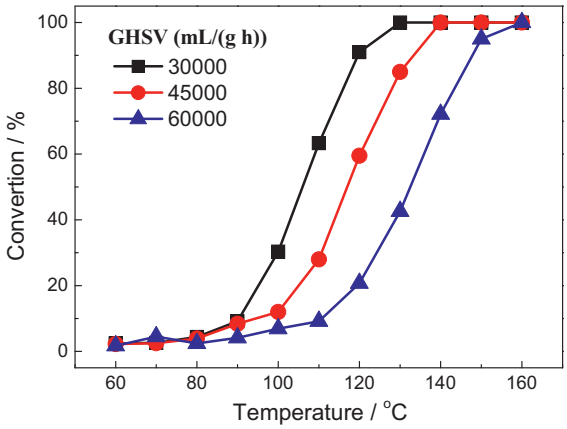

Fig. 3. Formaldehyde catalytic performance of different space velocity for 3D-Co_3O_4 catalyst under the conditions of HCHO concentration = 400 ppm, 20 vol% O_2, N_2 as balance gas.

3.2. Textural characterization of catalysts

The catalysts were characterized with XRD, N_2-physisorption and TEM. The wide-angle and low-angle XRD patterns of the Co_3O_4 catalysts are displayed in Fig. 5. The 3D-Co_3O_4 catalyst showed the (2 1 1), (2 2 0), and (3 3 2) diffraction peaks correspond to 1°, 1.14° and 1.85° (2θ) [31]. The peaks indicate that 3D-Co_3O_4 is a mesoporous material with a three-dimensional porous structure characteristic of the KIT-6 template (ia3d) [33,35]. The 2D-Co_3O_4 catalyst had (1 0 0) peak at 1° (2θ), which demonstrates that 2D-Co_3O_4 has the structural characteristics of SBA-15 (p6mm) mesoporous material [33]. The nano-Co_3O_4 showed no diffraction peak because it is a non-perforated material. From the wide-angle XRD image, the different Co_3O_4 catalysts all had diffraction peaks at 19°, 31.3°, 36.9°, 38.2°, 44.5°, 55.6°, 59.4° and 65.3° (2θ) [36],

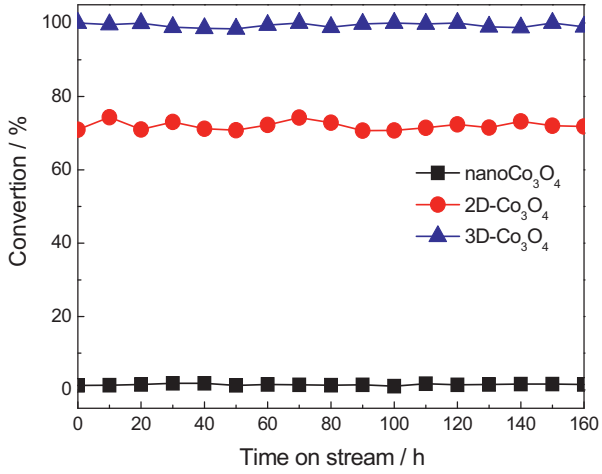

Fig. 4. Formaldehyde catalytic performance with time on stream over the different Co_3O_4 catalysts under the conditions of temperature = 130 °C, HCHO concentration = 400 ppm, 20 vol% O_2, N_2 as balance gas, GSHV = 30,000 mL/(g h).

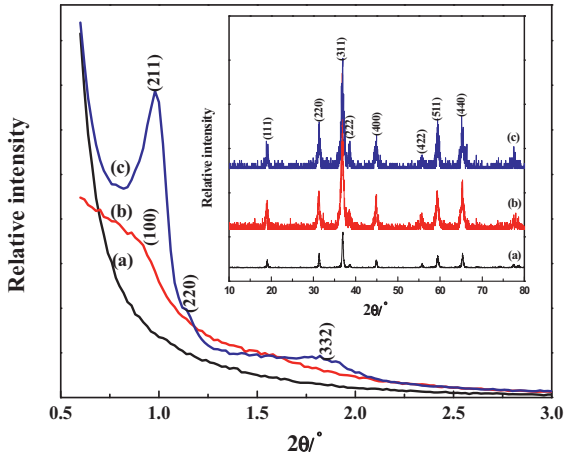

Fig. 5. Low-angle and wide-angle XRD patterns of the different Co_3O_4 catalysts: (a) nano-Co_3O_4, (b) 2D-Co_3O_4, (c) 3D-Co_3O_4.

corresponding to the (1 1 1), (2 2 0), (3 1 1), (2 2 2), (4 0 0), (4 2 2), (5 1 1) and (4 4 0) planes. The 3D-Co_3O_4 and 2D-Co_3O_4 prepared by the hard template method and the nano-Co_3O_4 synthesized by the precipitation method are all the crystalline cobalt oxide with spinel type structure.

The N_2 adsorption–desorption isotherm and the pore size distribution patterns of the mesoporous Co_3O_4 catalysts are shown in Fig. 6. The results of the N_2-physisorption demonstrate that the 2D-Co_3O_4 and 3D-Co_3O_4 materials exhibit the hysteresis phenomenon that belongs to the type IV isotherms, therefore, mesoporous structure present in the catalytic materials [35,37,38]. These results are consistent with the low-angle XRD image. The hysteresis ring of the 2D-Co_3O_4 is smaller than that of the 3D-Co_3O_4. Perhaps the 2D-Co_3O_4 and 3D-Co_3O_4 catalysts have different porous channel structures [18,31], thus the specific surface area of 3D-Co_3O_4 is larger than that of 2D-Co_3O_4. In addition, the type IV isotherm is less well defined for polycrystalline material. The isotherms are similar to those observed for other mesoporous transition metal oxides formed by hard template [38,39]. The hysteresis ring shapes of mesoporous Co_3O_4 catalysts are absolutely unlike mesoporous silicon as their hard template, which may be associated with a contribution from interparticle voids [39]. The BJH pore size distributions of mesoporous materials, calculated from the desorption

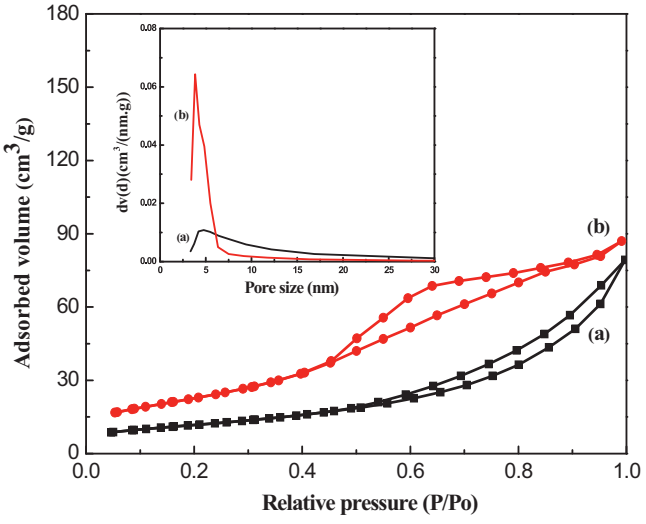

Fig. 6. N_2 Adsorption–desorption isotherm and pore size distributions of the mesoporous Co_3O_4 catalysts: (a) 2D-Co_3O_4, (b) 3D-Co_3O_4.

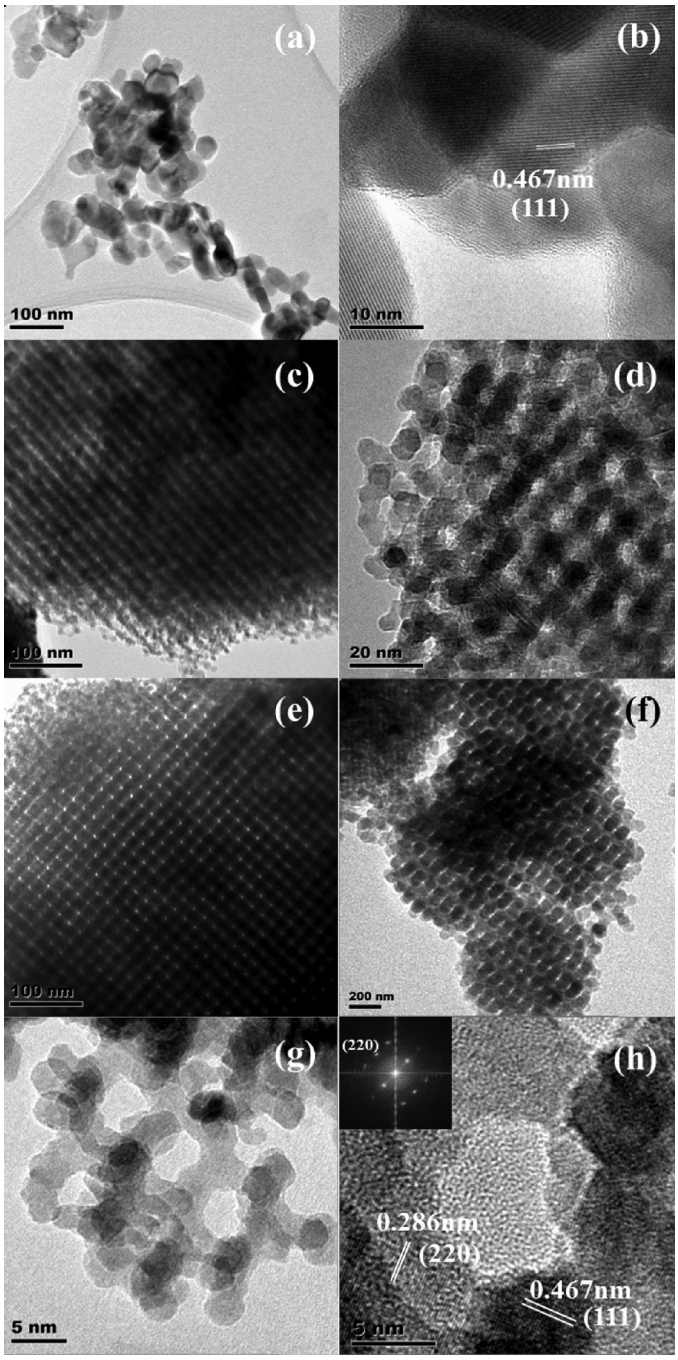

Fig. 7. TEM images of the different Co_3O_4 catalysts. The inset is the FFT diffractogram of the corresponding TEM image: (a and b) nano-Co_3O_4, (c and d) 2D-Co_3O_4, (e–h) 3D-Co_3O_4.

isotherms, show that the 2D-Co_3O_4 and 3D-Co_3O_4 have the mesoporous diameters of maximum distribution, 4.78 nm and 3.84 nm, respectively. This further indicates that 2D-Co_3O_4 and 3D-Co_3O_4 are a prefect replica structure of their templates. Pore structural parameters of the Co_3O_4 catalysts are displayed in Table 1. From the table, the BET surface areas of the mesoporous catalysts prepared by the hard template method are much larger, especially for 3D-Co_3O_4, than for the nano-Co_3O_4 (28.1 m^2/g) synthesized by the precipitation method. Moreover, 3D-Co_3O_4 has a 104.5 m^2/g BJH surface area, a 0.14 cm^3/g pore volume and a 3.84 nm pore diameter, and its large surface area is in agreement with the N_2-physisorption result.

Fig. 7 presents the transmission electron microscope images of the Co_3O_4 catalysts. From the chart, we can see that nano-Co_3O_4

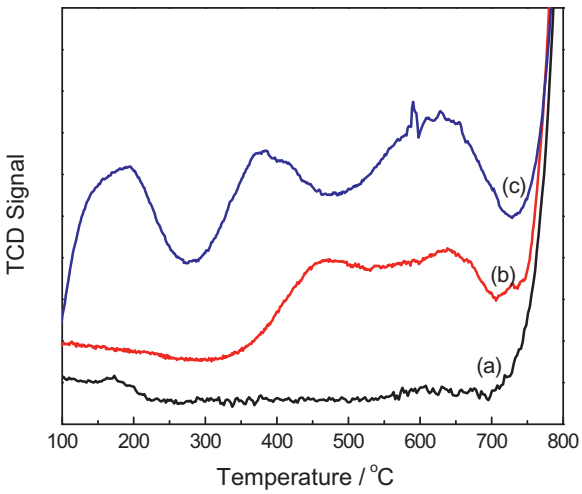

Fig. 8. O_2-TPD patterns of the different Co_3O_4 catalysts: (a) nano-Co_3O_4, (b) 2D-Co_3O_4, (c) 3D-Co_3O_4.

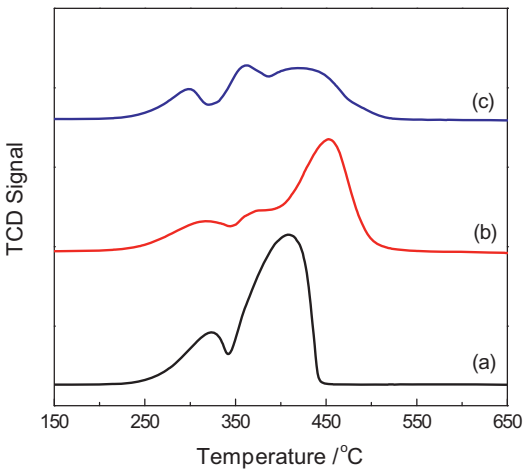

Fig. 9. H_2-TPR profiles of the different Co_3O_4 catalysts: (a) nano-Co_3O_4, (b) 2D-Co_3O_4, (c) 3D-Co_3O_4.

is composed of single crystals with no hole (Fig. 7a–b), whereas the 2D-Co_3O_4 and 3D-Co_3O_4 have polycrystalline hole walls. All of the catalysts show ordered mesopores (Fig. 7c–h) and retain the ordered structure of the SBA-15 or KIT-6 template. The hole showed by Fig. 7e–h of 3D-Co_3O_4 is more apparent, which is consistent with the result of the low-angle XRD result. The nano-Co_3O_4 has the (1 1 1) crystal plane with lattice spacing of 0.467 nm. The 3D-Co_3O_4 has the (1 1 1) crystal plane and the (2 2 0) crystal plane with lattice spacing of 0.286 nm. The top left corner in Fig. 7 h shows the fast Fourier transform (FFT) of mesoporous 3D-Co_3O_4 with [2 2 0] direction. The (1 1 1) crystal plane of nano-Co_3O_4 is not an active surface [25,31], whereas the (2 2 0) crystal plane in parallel with the (1 1 0) crystal plane is an active surface. According to the literature [25], the more active Co^{3+} species on the (1 1 0) faces of a Co_3O_4 nano-rod can easily oxidize CO, and the conventional Co_3O_4 nanoparticles had inferior CO oxidation activity because only Co^{2+} was exposed on the (0 0 1) and (1 1 1) faces. The nano-Co_3O_4 only exposes the (1 1 1) crystal faces, while the 3D-Co_3O_4 presents the (1 1 1) and (2 2 0) crystal planes. The (1 1 1) planes are composed of Co^{2+} ions which are not active sites, so nano-Co_3O_4 has the worst oxidation performance. The (2 2 0) crystal planes are mostly composed of abundant Co^{3+} species and these Co^{3+} ions on the exposed (2 2 0) faces provide sufficient active sites for the oxidation reaction, so 3D-Co_3O_4 catalyst shows excellent formaldehyde catalytic activity. Reactants were activated by Co^{3+} ions on the (2 2 0) facets when they diffused and adsorbed in the pores of 3D-Co_3O_4. Therefore, it is concluded that the number of Co^{3+} species on the exposed (2 2 0) facets is very important for oxidation reaction.

3.3. Thermal desorption behavior of catalysts

The O_2-TPD patterns of the different Co_3O_4 catalysts are shown in Fig. 8. Generally speaking, the oxygen species of the oxide are desorbed from easiest to hardest as follows: oxygen molecule (O_2) > oxygen molecule anion (O_2^-) > oxygen anion (O^-) > lattice oxygen (O^{2-}). O_2^- and O^- are molecular adsorption oxygen and surface chemical adsorption oxygen, respectively, and belong to the surface active oxygen, which is easy to desorb from the metal oxide. It is extremely difficult for lattice oxygen to desorb from the metal oxide catalysts [40,41]. Fig. 8 shows that desorption peaks that are less than 450 °C, between 450 °C and 700 °C, and more than 700 °C belong to the surface active oxygen, such as O_2^- and O^-, the surface lattice oxygen, and the bulk phase lattice oxygen, which all of the catalysts have, respectively. Except for the oxygen species greater than 700 °C, the nano-Co_3O_4 had almost no active oxygen. The 2D-Co_3O_4 had two desorption peaks but no peak at approximately 180 °C, which perhaps indicates a lack of O_2^- species. The 3D-Co_3O_4 catalyst presented three peaks, and the peak intensity was greater than for 2D-Co_3O_4, indicating that the 3D-Co_3O_4 surface has abundant surface active oxygen species (O_2^- and O^-). This phenomenon probably attributes to the lattice defect and oxygen vacancy that result from a larger specific surface area and three-dimensional channel structure of the 3D-Co_3O_4 sample. It is beneficial for oxygen in the gas phase to be activated and adsorbed onto the solid surface. According to the literature [31,42], the desorption temperature and intensity of catalytic materials is connected to their catalytic oxidation activity. Lower beginning oxygen desorption temperatures and larger intensities of desorption peaks lead to better catalytic ability. Therefore, 3D-Co_3O_4 has the best catalytic activity because of the abundance of active surface oxygen species that can easily participate in the catalytic oxidation reaction.

3.4. Thermal reduction behavior of catalysts

The H_2-TPR patterns of the different Co_3O_4 catalysts are illustrated in Fig. 9. The nano-Co_3O_4 shows two reduction peaks at 320 °C and 400 °C, which belong to the $Co^{3+} \rightarrow Co^{2+}$ (low temperature section) and $Co^{2+} \rightarrow Co^0$ (high temperature section). The low temperature reduction peak intensity of nano-Co_3O_4 is much smaller than its high temperature peak, which demonstrates that the quantity of Co^{2+} is greater than the quantity of Co^{3+}. The 2D-Co_3O_4 and 3D-Co_3O_4 have three reduction peaks at 300 °C, 380 °C and 450 °C. 300 °C peak belongs to the $Co^{3+} \rightarrow Co^{2+}$. The 380 °C and 450 °C peaks belong to $Co^{2+} \rightarrow Co^0$ oxidations. The reduction peak intensity at 300 °C for 3D-Co_3O_4 is greater than the intensity for 2D-Co_3O_4. It indicates that 3D-Co_3O_4 possesses greater quantity of Co^{3+}. Abundant Co^{3+} ions possibly increase the anionic defect position, which results from larger surface areas and special porous channels and is beneficial to catalytic oxidation. The literature reports that the quantity of Co^{3+} on the catalyst surface is correlated with catalytic activity [25,29,31].

3.5. Surface composition of the different Co_3O_4 catalysts

Fig. 10 is the Co and O X-ray photoelectron spectroscopy diagram of the different Co_3O_4 catalysts. Fig. 10A shows that O1s has signals displayed in BE at 529.8 and 531.3 eV. The reason is that the former is surface lattice oxygen (O_{latt}), whereas the latter is surface

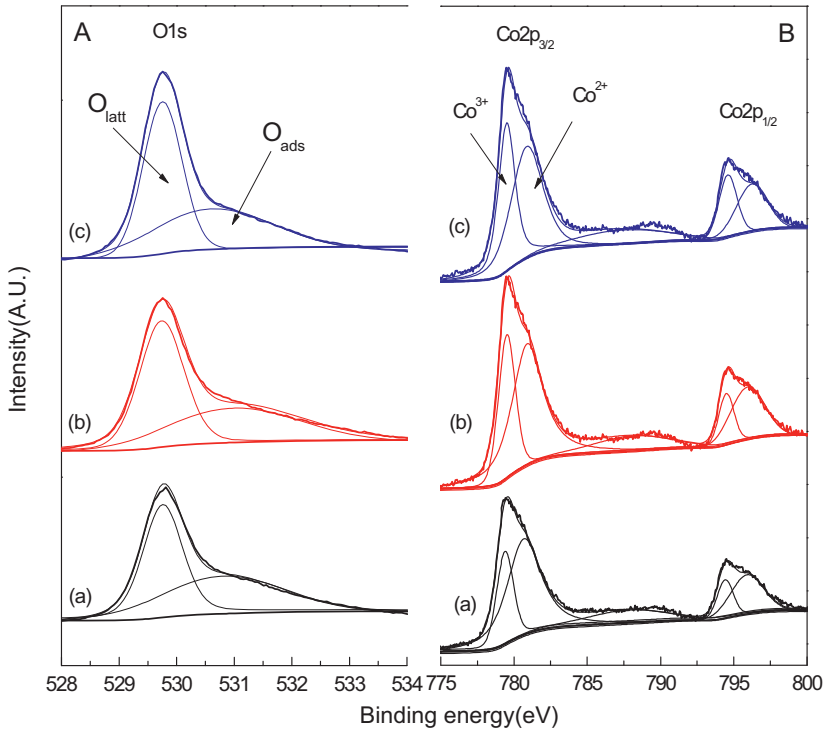

Fig. 10. XPS patterns of the different Co_3O_4 catalysts: (a) nano-Co_3O_4, (b) 2D-Co_3O_4, (c) 3D-Co_3O_4.

adsorption oxygen (O_{ads}) [43]. There is little difference between the two in the XPS analysis, 531.3–529.8 eV = 0.5 eV. Table 1 shows that there is little difference in the amount of surface adsorption oxygen and surface lattice oxygen between the catalysts. The O_{ads} of nano-Co_3O_4 is 48.2%, slightly greater than the mesoporous Co_3O_4, whereas O_{latt} is 51.8%, slightly less than the mesoporous Co_3O_4. The O_{ads} of 3D-Co_3O_4 is slightly larger than the mesoporous 2D-Co_3O_4, whereas the O_{latt} is slightly smaller than the 2D-Co_3O_4. The O_2-TPD results in Fig. 8 demonstrate that the reducing order of the contents of surface oxygen adsorption is 3D-Co_3O_4 > 2D-Co_3O_4 > nano-Co_3O_4. However, the XPS showed that the reducing order is nano-Co_3O_4 > 3D-Co_3O_4 > 2D-Co_3O_4. Because XPS can only quantify elements on the materials' surface, perhaps the pore structure and larger specific surface area of the mesoporous Co_3O_4 catalysts do not have an edge. However, if the channel structure and the larger specific surface area in the bulk phase of the mesoporous materials are taken into consideration, the reducing order of the surface oxygen adsorption should agree with the O_2-TPD test results. Fig. 10B shows that $Co2p_{3/2}$ has two components at BE = 778.9 and 781.3 eV and that $Co2p_{1/2}$ also has two in BE = 794.5 and 796.9 eV, [44] which are Co^{3+} and Co^{2+} ions, respectively. From Table 1, the reducing order on different Co_3O_4 catalysts' surfaces is 3D-Co_3O_4 > 2D-Co_3O_4 > nano-Co_3O_4. This result conforms to the H_2-TPR test results. If the channel structure and specific surface area in the bulk phase of the mesoporous catalysts is considered, there is likely more Co^{3+} total content than just the content of Co^{3+} ions on the surface. Therefore, mesoporous Co_3O_4, especially 3D-Co_3O_4, has a wealth of surface active oxygen species and Co^{3+} cationic species.

According to the characterization results, mesoporous Co_3O_4 catalysts, especially 3D-Co_3O_4, have the special pore structure, larger specific surface area, more abundant active surface oxygen species and active Co^{3+} cationic species on the exposed (2 2 0) crystal face. Xia et al. [43] considered that the activity of a catalyst was influenced by several factors, such as surface area, pore structure, surface oxygen species, active phase and reducibility. The special pore structure of mesoporous Co_3O_4 is favorable for the adsorption and diffusion of reactants and products. Compared with nano-Co_3O_4, 2D-Co_3O_4 and 3D-Co_3O_4 have the 2D and 3D ordered pore structure, respectively, which is beneficial to the increase of surface areas. The BET specific surface areas of 2D-Co_3O_4 and 3D-Co_3O_4 are 43.3 and 85.9 m^2/g, respectively, which are much larger than that of nano-Co_3O_4. A catalyst with larger specific surface area can expose more active facets in the oxidation reaction. TEM results show that the active faces of 3D-Co_3O_4 are the (2 2 0) crystal planes, which are mainly composed of abundant Co^{3+} ions which provide sufficient active sites for the oxidation reaction. More Co^{3+} ions are exposed on its surface, hence enhancing the catalytic ability further. H_2-TPR and XPS results reveal that greater quantities of Co^{3+} ions exist on the surface of the 3D-Co_3O_4, followed by the 2D-Co_3O_4. Moreover, much more Co^{3+} species can probably increase the anionic defects which are beneficial to the absorption and activation of oxygen in the gas phase. O_2-TPD results show that mesoporous Co_3O_4, particularly 3D-Co_3O_4, have more sufficient surface active oxygen species which are easily stripped and quickly filled by gas phase oxygen, and can improve the oxidation capacity. Surface active oxygen species play a crucial role in oxidation reaction [45]. For reaction mechanism of formaldehyde oxidation, Ma et al. [18] reported that the HCHO was first adsorbed on the Co_3O_4 (1 1 0) surface and formed the CHO surface species, meanwhile the Co^{3+} cations were reduced to Co^{2+}. The CHO species were oxidized by surface active oxygen to form $HCOO^-$ species, the Co^{2+} cations were simultaneously oxidized to Co^{3+}, and oxygen in the gas phase was activated. Then the $HCOO^-$ species were further oxidized to produce CO_2. The mechanism might be appropriate for the oxidation of formaldehyde on 3D-Co_3O_4 catalyst. Therefore, the overall catalytic performance of formaldehyde oxidation is related not only to the ratios of Co^{2+}/Co^{3+} and O_{ads}/O_{latt}, but also correlated to the pore structure, surface area and exposure of the lattice plane of (1 1 1) or (2 2 0). The structure and properties of 3D-Co_3O_4 are much more beneficial for formaldehyde oxidation, followed by the 2D-Co_3O_4.

4. Conclusions

The 2D-Co_3O_4 and 3D-Co_3O_4 catalysts were prepared by the hard template method, and the nano-Co_3O_4 catalyst was prepared by the precipitation method. The decrease order of the catalytic activity is 3D-Co_3O_4, 2D-Co_3O_4 and nano-Co_3O_4. The 3D-Co_3O_4 catalyst had the best formaldehyde catalytic oxidation performance, and the complete oxidation of formaldehyde occurred at 130 °C in space velocity of 30,000 mL/(g h). Characterization results showed that nano-Co_3O_4 was a nonporous structure with low specific surface area. The 2D-Co_3O_4 and 3D-Co_3O_4 retain the mesoporous characteristics and channel structures of the hard template and have large specific surface area, especially for 3D-Co_3O_4 with a three-dimensional channel structure. 3D-Co_3O_4 catalyst contains rich surface active oxygen species which are beneficial to formaldehyde oxidation, and more Co^{3+} cationic species on the surface which improves its oxidation ability. In addition, for 3D-Co_3O_4 catalyst, Formaldehyde conversion reached nearly 100% at 130 °C when space velocity is less than 30,000 mL/(g h), and complete conversion of formaldehyde had remained the same after 3D-Co_3O_4 was tested for 160 h. Therefore, the 3D-Co_3O_4 catalyst has the best catalytic activity and stability for formaldehyde, and it might be a potential non-noble catalyst in practical application.

Acknowledgments

The financial supports of the Science Fund for Creative Research Groups (Grant No. 21221004), the National High Science & Technology Project of China (Grant No. 2013AA065304) are gratefully acknowledged. This study was also supported by State Environmental Protection Key Laboratory of Sources and Control of Air Pollution Complex.

References

[1] T. Salthammer, S. Mentese, R. Marutzky, Chemical Reviews 110 (2010) 2536–2572.
[2] H. Huang, D.Y.C. Leung, Journal of Catalysis 280 (2011) 60–67.
[3] S.S. Kim, K.H. Park, S.C. Hong, Applied Catalysis A: General 398 (2011) 96–103.
[4] C. Zhang, F. Liu, Y. Zhai, H. Ariga, N. Yi, Y. Liu, K. Asakura, M. Flytzani-Stephanopoulos, H. He, Angewandte Chemie International Edition 51 (2012) 9628–9632.
[5] X. Yu, J. He, D. Wang, Y. Hu, H. Tian, Z. He, Journal of Physical Chemistry C 116 (2011) 851–860.
[6] N. An, Q. Yu, G. Liu, S. Li, M. Jia, W. Zhang, Journal of Hazardous Materials 186 (2011) 1392–1397.
[7] N. An, W. Zhang, X. Yuan, B. Pan, G. Liu, M. Jia, W. Yan, W. Zhang, Chemical Engineering Journal 215–216 (2013) 1–6.
[8] X. Tang, J. Chen, X. Huang, Y. Xu, W. Shen, Applied Catalysis B: Environmental 81 (2008) 115–121.
[9] Z. Huang, X. Gu, Q. Cao, P. Hu, J. Hao, J. Li, X. Tang, Angewandte Chemie International Edition 51 (2012) 4198–4203.
[10] Z.P. Qu, S.J. Shen, D. Chen, Y. Wang, Journal of Molecular Catalysis A: Chemical 356 (2012) 171–177.
[11] C.F. Mao, M.A. Vannice, Journal of Catalysis 154 (1995) 230–244.
[12] X. Tang, J. Chen, Y. Li, Y. Li, Y. Xu, W. Shen, Chemical Engineering Journal 118 (2006) 119–125.
[13] Y. Shen, X. Yang, Y. Wang, Y. Zhang, H. Zhu, L. Gao, M. Jia, Applied Catalysis B: Environmental 79 (2008) 142–148.
[14] J. Zhang, Y. Jin, C. Li, Y. Shen, L. Han, Z. Hu, X. Di, Z. Liu, Applied Catalysis B: Environmental 91 (2009) 11–20.
[15] H.F. Li, N. Zhang, P. Chen, M.F. Luo, J.Q. Lu, Applied Catalysis B: Environmental 110 (2011) 279–285.
[16] Y. Zhang, Y. Shen, X. Yang, S. Sheng, T. Wang, M.F. Adebajo, H. Zhu, Journal of Molecular Catalysis A: Chemical 316 (2010) 100–105.
[17] C. Li, Y. Shen, M. Jia, S. Sheng, M.O. Adebajo, H. Zhu, Catalysis Communications 9 (2008) 355–361.
[18] C. Ma, D. Wang, W. Xue, B. Dou, H. Wang, Z. Hao, Environmental Science and Technology 45 (2011) 3628–3634.
[19] B.C. Liu, Y. Liu, C.Y. Li, W.T. Hu, P. Jing, Q. Wang, J. Zhang, Applied Catalysis B: Environmental 127 (2012) 47–58.
[20] H. Huang, D.Y.C. Leung, ACS Catal. 1 (2011) 348–354.
[21] S.J. Park, I. Bae, I.S. Nam, B.K. Cho, S.M. Jung, J.H. Lee, Chemical Engineering Journal 195–196 (2012) 392–402.
[22] V.A. de la Pena O'Shea, M.C. Alvarez-Galvan, J.L.G. Fierro, P.L. Arias, Applied Catalysis B: Environmental 57 (2005) 191–199.
[23] R. Spinicci, M. Faticanti, P. Marini, S. De Rossi, P. Porta, Journal of Molecular Catalysis A: Chemical 197 (2003) 147–155.
[24] F. Wang, H. Dai, J. Deng, G. Bai, K. Ji, Y. Liu, Environmental Science and Technology 46 (2012) 4034–4041.
[25] X. Xie, Y. Li, Z. Liu, M. Haruta, W.J. Shen, Nature 458 (2009) 746–749.
[26] S.K. Meher, G.R. Rao, Journal of Physical Chemistry C 115 (2011) 15646–15654.
[27] Y. Yamada, K. Yano, Q. Xu, S. Fukuzumi, Journal of Physical Chemistry C 114 (2010) 16456–16462.
[28] M. Hilgendorff, B. Tesche, M. Giersig, Australian Journal of Chemistry 54 (2001) 497–501.
[29] L. Hu, Q. Peng, Y. Li, Journal of the American Chemical Society 130 (2008) 16136–16137.
[30] J. Yang, T. Sasaki, Crystal Growth and Design 10 (2010) 1233–1236.
[31] C. Ma, Z. Mu, J. Li, Y. Jin, J. Cheng, G. Lu, Z. Hao, S. Qiao, Journal of the American Chemical Society 132 (2010) 2608–2613.
[32] A. Rumplecker, F. Kleitz, E.L. Salabas, F. Schüth, Chemistry of Materials 19 (2007) 485–496.
[33] H. Tuysuz, C.W. Lehmann, H. Bongard, B. Tesche, R. Schmidt, F. Schuth, Journal of the American Chemical Society 130 (2008) 11510–11517.
[34] J. Li, C. Ma, X. Xu, J. Yu, Z. Hao, S. Qiao, Environmental Science and Technology 42 (2008) 8947–8951.
[35] F. Kleitz, F.O. Berube, R.M. Guillet-Nicolas, C.M. Yang, M. Thommes, Journal of Physical Chemistry C 114 (2010) 9344–9355.
[36] M. Casas-Cabanas, G. Binotto, D. Larcher, A. Lecup, V. Giordani, J.M. Tarascon, Chemistry of Materials 21 (2009) 1939–1947.
[37] C.E. Tattershall, N.P. Jerome, P.M. Budd, Journal of Materials Chemistry 11 (2001) 2979–2984.
[38] B. Lee, D. Lu, J.N. Kondo, K. Domen, Journal of the American Chemical Society 124 (2002) 11256–11257.
[39] F. Jiao, A. Harrison, J.C. Jumas, A.V. Chadwick, W. Kockelmann, P.G. Bruce, Journal of the American Chemical Society 128 (2006) 5468–5474.
[40] B.P. Barbero, J.A. Gamboa, L.E. Cadus, Applied Catalysis B: Environmental 65 (2006) 21–30.
[41] L. Xue, C. Zhang, H. He, Y. Teraoka, Applied Catalysis B: Environmental 75 (2007) 167–174.
[42] Z. Hao, D. Cheng, Y. Guo, Y. Liang, Applied Catalysis B: Environmental 33 (2001) 217–222.
[43] Y. Xia, H. Dai, H. Jiang, L. Zhang, Catalysis Communications 11 (2010) 1171–1175.
[44] J. Chen, Y. Zhang, L. Tan, Y. Zhang, Industrial and Engineering Chemistry Research 50 (2011) 4212–4215.
[45] H. Over, P.A. Seitsonen, Science 297 (2002) 2003–2005.